Continuation-based numerical detection of after-depolarisation and spike-adding threshold

Jakub Nowacki
jakub.nowacki@tessella.com
Tessella, 26 The Quadrant, Abingdon Science Park, Abingdon, OX14 3YS, UK

Hinke M. Osinga
h.m.osinga@auckland.ac.nz
Department of Mathematics,
The University of Auckland, Private Bag 92019, Auckland 1142, New Zealand

Krasimira T. Tsaneva-Atanasova
k.tsaneva-atanasova@bristol.ac.uk
Bristol Centre for Applied Nonlinear Mathematics,
Department of Engineering Mathematics,
University of Bristol, Queen's Building, University Walk, Bristol BS8 1TR, UK

The changes in neuronal firing pattern are signatures of brain function, and it is of interest to understand how such changes evolve as a function of neuronal biophysical properties. We address this important problem via the analysis and numerical investigation of a class of mechanistic mathematical models. We focus on a hippocampal pyramidal neuron model and study the occurrence of bursting related to the after-depolarisation (ADP) that follows after a brief current injection. This type of burst is a transient phenomenon, which is not amenable to the classical bifurcation analysis done, for example, for periodic bursting oscillators. In this paper, we show how to formulate such transient behaviour as a two-point boundary value problem (2PBVP), which can be solved using well-known continuation methods. The 2PBVP is formulated such that the transient response is represented by a finite orbit segment for which onsets of ADP and additional spikes in a burst can be detected as bifurcations during a one-parameter continuation. This, in turn, provides us with a direct method to approximate the boundaries of regions in a two-parameter plane where certain model behaviour of interest occurs. More precisely, we use two-parameter continuation of the detected onset points to identify the boundaries between regions with and without ADP, and bursts with different numbers of spikes. Our 2PBVP formulation is a novel approach to parameter sensitivity analysis that can be applied to a wide range of different problems.

1 Introduction

The firing patterns in neurons are an important feature that is generally associated with specific brain functions (Llinás, 1988). Under various conditions, many neurons tend to fire bursts, i.e., clusters of high-frequency spikes (Krahe & Gabbiani, 2004). Bursts are generated in response to stimuli, which can be electrical (Yue & Yaari, 2004; Brown & Randall, 2009) or chemical (Rinzel, 1985; Tsaneva-Atanasova, Sherman, van Goor, & Stojilkovic, 2007) and occur periodically or as single events. The bursting activity is characterised by slow alterations between near-steady-state behaviour, the so-called silent phase, and the active phase when clusters of spikes are fired (Rinzel, 1987). This bursting behaviour plays an important role in many phenomena, namely, synaptic plasticity (Thomas, Watabe, Moody, Makhinson, & O'Dell, 1998), transmission of stimulus-related information (Krahe & Gabbiani, 2004) and sensory system function (Martinez-Conde, Macknik, & Hubel, 2002). It is not only limited to controlled in-vitro experiments, but has also been reported to occur in-vivo. For instance, spiking and bursting behaviour has been documented in in-vivo recordings from a single place cell (Lee, Manns, Sakmann, & Brecht, 2006; Harvey, Collman, Dombeck, & Tank, 2009; Epsztein, Brecht, & Lee, 2011). In addition, such firing patterns are reported to take place in pathological conditions such as epilepsy (McCormick & Contreras, 2001) and Alzheimer's disease (Brown et al., 2011). Even relatively small changes in biophysical properties of neurons (Brown & Randall, 2009; Nowacki, Osinga, Brown, Randall, & Tsaneva-Atanasova, 2011; Brown, Chin, Leiser, Pangalos, & Randall, 2011) or their morphology (Van Elburg & Van Ooyen, 2010) can have a large impact on the neuron's excitable behaviour. Therefore, when using mathematical models for studying such firing patterns, it is essential to consider different sets of parameters, as parameter uncertainty is common in these models.

We present a method that allows for the analysis of transient processes. In contrast to periodic bursting, transients bursts are challenging to address with standard bifurcation methods, which are designed for long-term behaviour. Periodic bursters, also called bursting oscillators, have been studied extensively; for example, see (Rinzel, 1987; Terman, 1991; Guckenheimer, Gueron, & Harris-Warrick, 1993; Izhikevich, 2000; Govaerts & Dhooge, 2002; Guckenheimer, Tien, and Willms, 2005; Tsaneva-Atanasova, Osinga, Rieß, & Sherman, 2010; Ermentrout & Terman, 2010). Here, a parameter-driven modification of firing patterns, such as spike adding, is associated with so-called fold bifurcations of these periodic orbits (Terman, 1991; Tsaneva-Atanasova et al., 2010). In this paper, we are interested in spike adding and bursting as a transient behaviour, which is known to occur, e.g., in hippocampal pyramidal neurons (Andersen et al., 2007; Brown & Randall, 2009; Nowacki et al., 2011). In this case, a neuron is stimulated briefly, that is, perturbed away from its resting potential, and bursting takes place during the return to this equilibrium state. Due to the uniqueness of solutions in deterministic systems, the firing patterns that arise from prescribed perturbations away from equilibrium cannot coexist. Hence, parameter-driven modifications, such as spike adding cannot be associated with fold bifurcations of periodic orbits, and classical bifurcation methods used for identifying different bursting patterns in mathematical models,

cannot be applied in the context of transient behaviour. Nevertheless, the underlying spike-adding mechanism via a canard-like phase is the same as for periodic orbits. Indeed, we already presented a detailed slow-fast analysis of this behaviour using elements of Geometric Singular Perturbation Theory (Nowacki, Osinga, & Tsaneva-Atanasova, 2012).

In this paper, we focus on the numerical detection of transient firing patterns in our system. We show how one can associate a type of bifurcation or sequence of bifurcations with the phenomenon of spike adding in a transient burst. As in (Nowacki et al., 2012), we view the response of the system to a short current injection as a finite-time orbit segment that is the solution of a two-point boundary value problem (2PBVP). The parameter dependence of such solutions can then be studied via the numerical continuation of the solutions to this 2PBVP. The 2PBVP set-up used in our approach is quite general and can be applied to many transient bursting patterns. Our primary motivation for developing this method is to study transient bursting related to so-called after-depolarisation (ADP) and how it depends on neuronal biophysical properties. The phenomenon of ADP is empirically defined as a positive deflection of the membrane potential after a spike, which creates a characteristic 'hump' (Izhikevich, 2006). A series of additional spikes on top of ADP are generated if the membrane potential crosses a bursting threshold during the ADP (Brown & Randall, 2009; Nowacki et al., 2011). In this paper, we consider the ADP to be the positive deflection of the membrane potential after the last spike triggered by the short current injection. We use the 2PBVP formulation to define the onsets of ADP and a spike, such that these onsets can be detected as fold bifurcations in a one-parameter continuation of the 2PBVP. A subsequent two-parameter fold continuation establishes curves in a two-parameter plane that approximate the boundaries between regions of different bursting behaviours in the model, and identifies the excitability threshold.

We consider a model of pyramidal neurons as a case study to illustrate the approximation of onsets of ADP and bursts with our numerical method. This case study is a bursting neuron model that uses four general classes of fast and slow, inward and outward currents in Hodgkin-Huxley formalism (Hodgkin & Huxley, 1952) and has been systematically derived via careful comparison to a detailed pyramidal cell model (Nowacki et al., 2011). The main feature that we exploit in our study is a natural time-scale separation in the model. The majority of classical work on periodic spiking and bursting behaviour, such as (Rinzel, 1987; Terman, 1991; Guckenheimer et al., 1993; Izhikevich, 2000), emphasises the pivotal role of the slow variables for governing these behaviours. We find that we can also make use of this time-scale separation when characterising the onset of ADP or the threshold for a new spike. Indeed, both onsets of ADP and a spike can be approximated as extrema of a slow variable of the system. We explain in detail how to formulate the problem such that one can detect the extremum as a fold bifurcation with respect to a system variable, which is not achievable using the standard fold detection with respect to parameters. As a result, we are able to perform a one-parameter fold detection and two-parameter fold continuation of the 2PBVP over a large region of interest in the two-parameter plane. The advantage of our approach is that the numerical method automatically identifies a parameter-dependent and

state-dependent excitability threshold as part of the computation.

Parameter continuations may be particularly important for model predictions that take into account the effects of parameters that currently cannot be controlled in an experimental environment. Our approach is very effficient, because we characterise the boundaries between regions of ADP and other excitable behaviour in such a way that they can be detected directly and continued numerically in a two-parameter setting. This means that we compute the boundary explicitly as a one-dimensional curve, rather than identifying it implicitly in a brute-force exploration of the entire two-parameter plane. Based on our analysis we are able to describe the implications of changes to model parameters for excitability.

This paper is organised as follows. In the next section, we present our model of study. In Section 3, we formulate the problem as a 2PBVP and show how to constrain the system such that the solutions correspond to those at a threshold. We discuss both the onsets of ADP and a spike in Sections 3.1 and 3.2, respectively, and show how to detect these as folds in a one-parameter continuation. We continue these folds in two parameters in Section 4 and obtain an overview of the regions of different model behaviours. We then provide a detailed investigation of the model behaviour at and near the boundaries of these regions. We end with conclusions in Section 5. The numerical computations are performed with the package AUTO (Doedel, 1981; Doedel & Oldeman, 2009) and visualisations are done in Python (Oliphant, 2007) using Matplotlib (Hunter, 2007).

2 The model

We use the model from Nowacki et al. (2012) as a case study to illustrate our new numerical method for detection and subsequent continuation of the onsets of ADP or a spike. This model is a simplified version of the physiological model of hippocampal pyramidal neurons presented in (Nowacki et al., 2011), and considers general classes I_{FI}, I_{SI}, I_{FO} and I_{SO} of fast and slow, inward and outward currents in Hodgkin-Huxley formalism (Hodgkin & Huxley, 1952). The model is five dimensional and has the form

$$\begin{cases} \dfrac{dV}{dt} &= \dfrac{1}{C_{\mathrm{m}}}\left[-g_{\mathrm{FI}}\, m_{\mathrm{FI}_\infty}(V)\,(V-E_{\mathrm{I}}) - g_{\mathrm{SI}}\, m_{\mathrm{SI}}^2\, h_{\mathrm{SI}}\,(V-E_{\mathrm{I}}),\right. \\ & \qquad \left. -g_{\mathrm{FO}}\, m_{\mathrm{FO}}\,(V-E_{\mathrm{O}}) - g_{\mathrm{SO}}\, m_{\mathrm{SO}}\,(V-E_{\mathrm{O}}) + I_{\mathrm{app}}\right] \\ \dfrac{dx}{dt} &= \dfrac{x_\infty(v)-x}{\tau_x}, \end{cases} \tag{2.1}$$

where $x \in \{m_{\mathrm{SI}}, m_{\mathrm{FO}}, m_{\mathrm{SO}}, h_{\mathrm{SI}}\}$; here, we assume that the fast inward current is instantaneous. We use the Boltzmann form

$$x_\infty(v) = \frac{1}{1+\exp\left(-\frac{V-V_x}{k_x}\right)}, \tag{2.2}$$

Table 1: Default parameter values for the simplified pyramidal neuron model (2.1).

	$C_\mathrm{m} = 1.0\,\mu\mathrm{F/cm}^2$							
	Inward currents:				Outward currents:			
	E_I	$=$	80.0	mV	E_0	$=-80.0$	mV	
Fast:	g_FI	$=$	2.0	$\mathrm{mS/cm}^2$				
	$V_{\mathrm{m_{FI}}}$	$=-25.0$		mV				
	$k_{\mathrm{m_{FI}}}$	$=$	5.0	mV				
	g_SI	$=$	0.5	$\mathrm{mS/cm}^2$	g_FO	$=$	9.5	$\mathrm{mS/cm}^2$
	$V_{\mathrm{m_{SI}}}$	$=-54.0$		mV	$V_{\mathrm{m_{FO}}}$	$=$	-6.0	mV
	$k_{\mathrm{m_{SI}}}$	$=$	5.0	mV	$k_{\mathrm{m_{FO}}}$	$=$	11.5	mV
	$\tau_{\mathrm{m_{SI}}}$	$=$	3.0	ms	$\tau_{\mathrm{m_{FO}}}$	$=$	1.0	ms
Slow:					g_SO	$=$	1.2	$\mathrm{mS/cm}^2$
	$V_{\mathrm{h_{SI}}}$	$=-56.0$		mV	$V_{\mathrm{m_{SO}}}$	$=-20.0$	mV	
	$k_{\mathrm{h_{SI}}}$	$=$	8.5	mV	$k_{\mathrm{m_{SO}}}$	$=$	10.0	mV
	$\tau_{\mathrm{h_{SI}}}$	$=$	20.0	ms	$\tau_{\mathrm{m_{SO}}}$	$=$	75.0	ms

for the relevant activation and inactivation steady-state functions $m_{\mathrm{FI}_\infty}(V)$, $m_{\mathrm{SI}_\infty}(V)$, $m_{\mathrm{FO}_\infty}(V)$, $m_{\mathrm{SO}_\infty}(V)$, and $h_{\mathrm{SI}_\infty}(V)$. The parameters used are the same as in (Nowacki et al., 2012), unless specified otherwise; these default values are also given in Table 1, for convenience.

System (2.1) is capable of reproducing a broad range of cell responses typically observed in experiments; see (Nowacki et al., 2011) and also (Brown & Randall, 2009; Golomb, Yue, & Yaari, 2006; Yue, Remy, Su, Beck, & Yaari, 2005). Here, we mimic the experiment where a current is injected for only a short time. If the injected current is strong enough then one or more spikes are generated during the transient phase, where the system returns to its resting potential. For our numerical experiment, we set $I_{app} = 20\,\mu\mathrm{A/cm}^2$ and apply it to system (2.1) over a time interval of 3 ms, which ensures that the membrane potential V rises to a fully developed spike before the current is turned off.

Figure 1(a) depicts the time series of V for three such experiments, where the conductance g_SI of the slow inward current is set to the three successive values of 0.15, 0.40 and $0.60\,\mathrm{mS/cm}^2$. The injected current is applied at $t = 20$ ms and the resulting first spike is almost the same for each of the three responses. However, the subsequent behaviour, after the applied current has been turned off, clearly depends on the choice of g_SI. The responses for $g_\mathrm{SI} = 0.40\,\mathrm{mS/cm}^2$ (middle curve) and $g_\mathrm{SI} = 0.60\,\mathrm{mS/cm}^2$ (top curve) exhibit ADP, while the response for $g_\mathrm{SI} = 0.15\,\mathrm{mS/cm}^2$ (bottom curve) is a spike without ADP.

The occurrence of ADP can easily be defined as a crossing of the V-nullcline (Nowacki et al., 2011); we illustrate this in Figure 1(b), where we plot the responses in the projection onto the $(dV/dt,\, V)$-plane and focus on the activity near the V-nullcline, that is, the vertical dashed line at $dV/dt = 0$. As explained previously (Nowacki et al., 2011), at the onset of ADP, the membrane potential has a cubic tangency, which means that the response, when projected onto the $(dV/dt, V)$-plane, makes a quadratic tangency with the V-nullcline. The

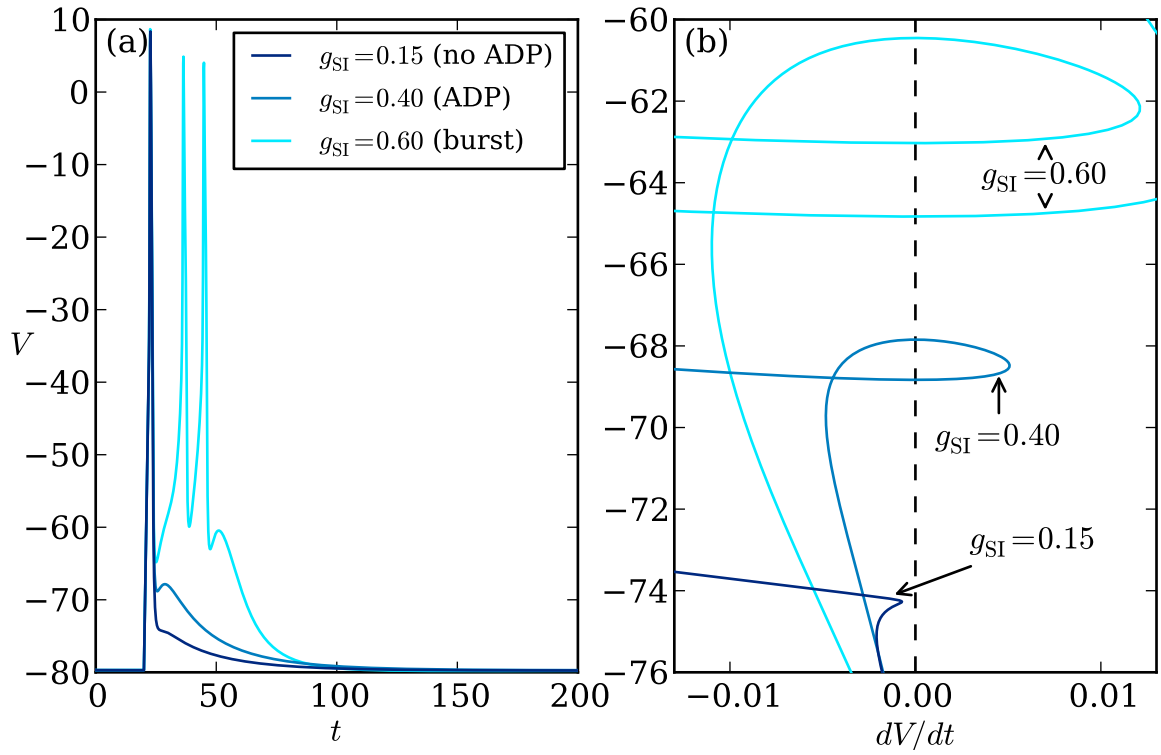

Figure 1: Three responses of system (2.1) to a current injection applied at $t = 20\,\text{ms}$ of strength $I_{app} = 20\,\mu\text{A/cm}^2$ and duration 3 ms, where g_{SI} (in mS/cm^2) takes the values $g_{\text{SI}} = 0.15$, $g_{\text{SI}} = 0.40$ and $g_{\text{SI}} = 0.60$. Panel (a) shows the resulting time series of the membrane potential V and panel (b) an enlargement in the $(dV/dt, V)$-plane of the region of interest near the V-nullcline (vertical dashed line).

response without ADP, for $g_{\text{SI}} = 0.15\,\text{mS/cm}^2$, lies entirely to the left of the V-nullcline in Figure 1(b), while the (middle) response for $g_{\text{SI}} = 0.40\,\text{mS/cm}^2$ exhibits a non-monotonic loop and $dV/dt > 0$ during the short rise time of ADP. A second cubic tangency develops as g_{SI} increases from $0.40\,\text{mS/cm}^2$ to $0.60\,\text{mS/cm}^2$, so that the response for $g_{\text{SI}} = 0.60\,\text{mS/cm}^2$ in Figure 1(b) crosses the V-nullcline multiple times; note that the ADP after the last spike is qualitatively the same as that for $g_{\text{SI}} = 0.40\,\text{mS/cm}^2$.

The presence of ADP is a precursor for generating a spike and we expect that the respective onsets of ADP and a new spike occur close together in parameter space. In the next section, we explain how to detect both onsets numerically.

3 Excitability thresholds as a boundary value problem

We formulate the onset of ADP and the thresholds of each new spike in a burst as two-point boundary value problems (2PBVP) in such a way that a standard numerical continuation

package can be used. We implemented our approach using AUTO (Doedel, 1981; Doedel & Oldeman, 2009), but other continuation packages, such as the recently developed package CoCo (Dankowicz & Schilder, 2009, 2011), would be suitable as well.

We remark here that the set-up in AUTO is rather similar to the computational approach taken in (Nowacki et al., 2012), but there is an important difference in the definition of the boundary conditions. In (Nowacki et al., 2012) we analysed the geometrical mechanism of spike adding and investigated how the transient response of system (2.1) was tracing the slow manifolds of the underlying fast subsystem. Since the transitions between responses with a different number of spikes occur over exponentially small parameter intervals, we used 2PBVP continuation to capture the topological changes of the response, which would be virtually impossible to compute using initial-value integration. However, the 2PBVP set-up in (Nowacki et al., 2012) does not identify the moment of the spike-adding transitions; it only characterises these transitions from a geometrical point of view. For completeness, we formulate the 2PBVP again here, and point the reader who is familiar with the set-up in (Nowacki et al., 2012) to the difference in formulating the boundary conditions (3.6) in Section 3.1 and (3.7) in Section 3.2 that determine the total integration time for the orbit segment, respectively.

As is standard in AUTO, we consider an orbit segment $\mathbf{u} = \mathbf{u}(t)$ defined on the time interval $0 \leq t \leq 1$. For $t \in [0,1]$, we define $\mathbf{u}(t) = [V(t\,T),\, m_{\rm SI}(t\,T),\, m_{\rm FO}(t\,T),\, m_{\rm SO}(t\,T),\, h_{\rm SI}(t\,T)]$ as the five-dimensional phase-space vector in system (2.1), which is a solution of

$$\mathbf{u}' = T\,\mathbf{f}(\mathbf{u}, \lambda, I_{\rm app}). \tag{3.1}$$

Here, $\mathbf{f} : \mathbb{R}^5 \times \mathbb{R}^k \times \mathbb{R}$ is the continuously differentiable right-hand side of system (2.1). The time rescaling to the $[0,1]$-interval has the effect that the total required integration time T appears as a parameter in (3.1); see also (Nowacki et al., 2012). The parameter vector $\lambda \in \mathbb{R}^k$ essentially represents the parameters of interest; we focus on the maximal conductances $g_{\rm SI}$ and $g_{\rm FO}$ of the slow inward and fast outward currents. However, additional parameters will be introduced to obtain a well-posed 2PBVP, so that λ typically consists of more than two parameters. The applied current $I_{\rm app}$ is specified separately in (3.1) and we consider two consecutive orbit segments, denoted $\mathbf{u}_{\rm ON}$ and $\mathbf{u}_{\rm OFF}$, such that $\mathbf{u}_{\rm ON}$ satisfies (3.1) with $I_{\rm app} = 20\,\mu{\rm A/cm^2}$ and $\mathbf{u}_{\rm OFF}$ satisfies (3.1) with $I_{\rm app} = 0\,\mu{\rm A/cm^2}$.

More precisely, we consider the system of equations

$$\mathbf{u}'_{\rm ON}(t) = T_{\rm ON}\ \mathbf{f}(\mathbf{u}_{\rm ON}(t), \lambda, I_{\rm app}), \tag{3.2}$$

$$\mathbf{u}'_{\rm OFF}(t) = T_{\rm OFF}\,\mathbf{f}(\mathbf{u}_{\rm OFF}(t), \lambda, 0), \tag{3.3}$$

where the end point $\mathbf{u}_{\rm ON}(1)$ of $\mathbf{u}_{\rm ON}$ is the starting point $\mathbf{u}_{\rm OFF}(0)$ of $\mathbf{u}_{\rm OFF}$. That is, we require the boundary condition

$$\mathbf{u}_{\rm ON}(1) - \mathbf{u}_{\rm OFF}(0) = 0. \tag{3.4}$$

The short current injection is supposed to perturb system (3.1) from its resting potential. Hence, the begin point $\mathbf{u}_{\rm ON}(0)$ of $\mathbf{u}_{\rm ON}$ should be equal to the stable equilibrium of (3.1) with

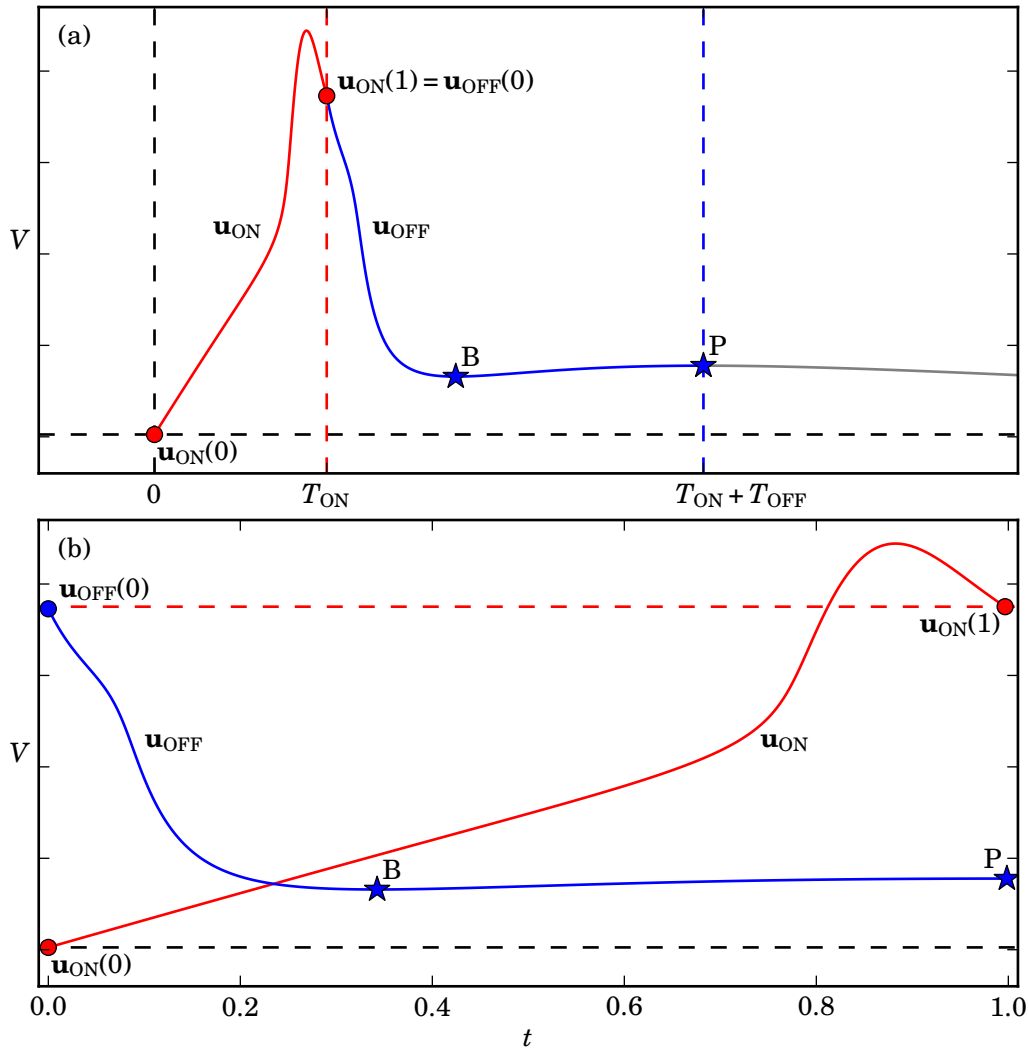

Figure 2: Illustration of how to interpret solutions to the 2PBVP (3.2)–(3.5); shown is a solution of (2.1) for which the short current injection generates a single spike and the transient response only generates an ADP. Panel (a) shows the time series of V for the concatenated orbit segments $\mathbf{u}_{\rm ON}$ and $\mathbf{u}_{\rm OFF}$ rescaled back to original time. The corresponding numerical representation on the $[0, 1]$-interval is shown in panel (b). The first (red) segment $\mathbf{u}_{\rm ON}$ starts at the resting potential for $I_{\rm app} = 0\,\mu{\rm A/cm}^2$, as indicated by the horizontal dashed line, and is a solution of equation (3.2) with $I_{\rm app} = 20\,\mu{\rm A/cm}^2$; the total integration time is $T_{\rm ON}$, which we set to 3 ms. The second (blue) segment $\mathbf{u}_{\rm OFF}$ starts at the end point $\mathbf{u}_{\rm ON}(1)$ of $\mathbf{u}_{\rm ON}$ and is a solution of equation (3.3) with total integration time $T_{\rm OFF}$. As explained in Section 3.1, we define $T_{\rm OFF}$ such that $\mathbf{u}_{\rm OFF}(1)$ lies at the local maximum, denoted P.

$I_{\text{app}} = 0$, which we can solve for implicitly by imposing the boundary condition

$$\mathbf{f}(\mathbf{u}_{\text{ON}}(0), \lambda, 0) = 0. \tag{3.5}$$

Note that system (3.2)–(3.3) with boundary conditions (3.4) and (3.5) is effectively an initial value problem that has a well-defined unique solution as soon as the two integration times T_{ON} and T_{OFF} have been specified. The nature of the short current injection is such that T_{ON} is fixed (we set $T_{\text{ON}} = 3\,\text{ms}$). The idea is to restrict T_{OFF} in such a way that the solution to (3.2)–(3.5) is determined by the onset of ADP or the onset of a spike. Indeed, both ADP and additional bursting take place after the current has been switched off, hence, they are a characterisation of the orbit segment $\mathbf{u}_{\text{OFF}}$. Figure 2 illustrates the set-up with an example where we defined $\mathbf{u}_{\text{OFF}}$ with the additional constraint that $\mathbf{u}_{\text{OFF}}(1)$ lies at a local maximum, denoted P; this local maximum P is preceded by a local minimum, denoted B, and indicates the presence of ADP. The concatenation of $\mathbf{u}_{\text{ON}}$ and $\mathbf{u}_{\text{OFF}}$ in original time coordinates is shown with the time series of V in Figure 2(a). This combined trajectory is a solution of system (2.1) with I_{app} following the short-current-injection protocol. We only consider the trajectory in Figure 2 (a) up to time $T_{\text{ON}} + T_{\text{OFF}}$; the grey line indicates the extended trajectory over a longer time interval. Figure 2(b) shows the two orbit segments $\mathbf{u}_{\text{ON}}$ and $\mathbf{u}_{\text{OFF}}$ with time rescaled to the $[0, 1]$-interval.

The boundary conditions that determine T_{OFF} at the onset of ADP or the onset of a new spike are explained and illustrated in the next two sections. We do not describe here how to obtain a first solution to such 2PBVPs; this has been discussed in detail for a similar 2PBVP in Nowacki et al. (2012). Note that a different first solution must be generated each time when detecting the next onset of ADP or the next onset of a new spike.

3.1 Identifying the onset of ADP in a transient burst

The ADP is characterised by the existence of a local minimum B and a local maximum P, which occur after one or a series of spikes and form a small hump as shown in Figure 2(a). The 2PBVP (3.2)–(3.5) has a solution that corresponds to a response with ADP, if we restrict T_{OFF} such that the orbit segment $\mathbf{u}_{\text{OFF}}$ ends at P, that is, $\mathbf{u}_{\text{OFF}}$ ends precisely at the point where it has a local maximum with respect to V. Hence, we do not fix the integration time T_{OFF} for $\mathbf{u}_{\text{OFF}}$, but determine its value by requiring $dV/dt = 0$ at $\mathbf{u}_{\text{OFF}}(1)$. This can be expressed as the boundary condition

$$f_1(\mathbf{u}_{\text{OFF}}(1), \lambda, 0) = 0, \tag{3.6}$$

where f_1 is the first equation of system (2.1), that is, the equation for dV/dt.

Figure 3 shows six solutions selected from the family of orbit segments that is obtained by continuation of the 2PBVP (3.2)–(3.6) using g_{SI} as the free parameter; here, we decreased g_{SI} from $g_{\text{SI}} = 0.5\,\text{mS/cm}^2$. Figure 3(a) shows the time series of V scaled back to the original time; see also Figure 2(a). The variation in g_{SI} has almost no effect on the orbit segment $\mathbf{u}_{\text{ON}}$ of (3.2) that satisfies (3.5) with $T_{\text{ON}} = 3\,\text{ms}$, so that $\mathbf{u}_{\text{OFF}}$ starts at almost the same

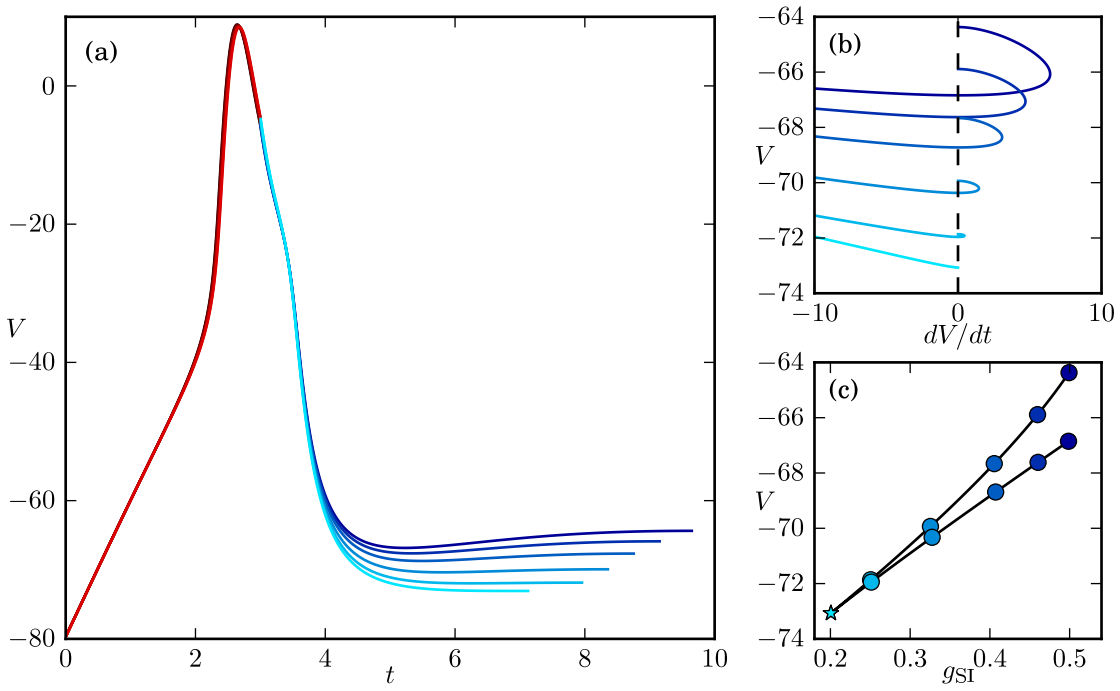

Figure 3: Continuation of the 2PBVP (3.2)–(3.6) as $g_{\rm SI}$ decreases. Panel (a) shows selected time series in V of the $g_{\rm SI}$-dependent solutions; the lowest orbit segment corresponds to the smallest value of $g_{\rm SI}$ and is the response at the onset of ADP. Panel (b) shows an enlargement near the V-nullcline (vertical dashed line) of these solutions projected onto the (dV/dt, V)-plane and clearly shows that all end points satisfy $dV/dt = 0$; the lowest orbit segment is again at the onset of ADP. Panel (c) shows the value of V for each point $\mathbf{u}_{\rm OFF}(t)$ that satisfies $dV/dt = 0$, illustrating that the lowest orbit segment in panels (a) and (b) corresponds to a fold (marked by the blue star), where $g_{\rm SI}$ is minimal.

point for all these orbit segments. However, the end points of $\mathbf{u}_{\rm OFF}$ change substantially, and the value for $T_{\rm OFF}$ decreases with $g_{\rm SI}$, which also corresponds to a decrease in the value of the V-coordinate. Figure 3(b) shows only the orbit segments $\mathbf{u}_{\rm OFF}$ in projection onto the (dV/dt, V)-plane, where we focus on the parts near the end points $\mathbf{u}_{\rm OFF}(1)$; as before, the value of the V-coordinate decreases with $g_{\rm SI}$. The local minima B and maxima P that indicate the existence of ADP are the points on $\mathbf{u}_{\rm OFF}$ with $dV/dt = 0$, which is the vertical dashed line in Figure 3(b). Since we require (3.6), all end points $\mathbf{u}_{\rm OFF}(1) = P$ satisfy $dV/dt = 0$. Note that the local minima B also lie on the V-nullcline, so that each selected orbit segment also intersects the line $dV/dt = 0$ at a point $\mathbf{u}_{\rm OFF}(t) = B$ with $0 < t < 1$. The only exception is the lowest orbit segment in Figure 3(b); this orbit segment corresponds to the solution of (3.2)–(3.6) for which the continuation reaches a

minimum value of $g_{\mathrm{SI}} \approx 0.2006\,\mathrm{mS/cm^2}$, and at this parameter value AUTO detects a fold bifurcation (Kuznetsov, 1998). This is visualised in Figure 3(c), where we plot the V-coordinates of the points B and P for each of the orbit segments $\mathbf{u}_{\mathrm{OFF}}$. The bifurcation diagram in Figure 3(c) illustrates how the continuation of the local maximum P turns into a continuation of the local minimum B as g_{SI} increases past the fold bifurcation (marked by a star); the upper branch in Figure 3(c) corresponds to orbit segments that end at points P and the lower branch to orbit segments that end at points B. The fold bifurcation itself corresponds to an inclination point at which B and P merge, which means that it marks the onset of ADP; note that the fold bifurcation seems to lie at a cusp point, but this is an artefact of the projection and the computed branch is actually a smooth curve.

We remark here that fold bifurcations can be detected automatically during a one-parameter continuation run with the set-up in AUTO. Furthermore, any detected fold bifurcation can be continued directly using a second parameter. Hence, our approach allows us to trace the onset of ADP as a curve in two parameters.

3.2 Identifying the onset of a spike in a transient burst

Decreasing g_{SI} in Section 3 led to an onset of ADP at the minimum value $g_{\mathrm{SI}} \approx 0.2006\,\mathrm{mS/cm^2}$. On the other hand, we expect that increasing g_{SI} leads to the onset of a spike from the ADP. More precisely, we expect that the peak P of ADP will rise until it reaches some critical threshold value of the membrane potential V; indeed, classical studies of excitability tend to associate the excitability threshold with a certain value of the membrane potential (Hodgkin & Huxley, 1952; Izhikevich, 2006; Keener & Sneyd, 2008). Hence, the natural approach would be to monitor the value of V at the end point $\mathbf{u}_{\mathrm{OFF}}(1)$ in system (3.2)–(3.6) and define the onset of a burst as the point where g_{SI} is such that $\mathbf{u}_{\mathrm{OFF}}(1)$ has reached the critical threshold of the membrane potential. There is a major disadvantage to this idea, namely, one would have to guess what the value of the critical threshold actually is and make heuristic assumptions, for example, that the critical threshold does not depend on g_{SI}. Here, we explore a different approach to define the onset of a spike, which automatically establishes the critical threshold at the same time.

As explained in (Nowacki et al., 2012), the critical threshold is characterised by a response with an elongated depolarised state of maximal duration. Nevertheless, the actual generation of a new spike takes place over an exponentially small g_{SI}-interval. The first such spike generation occurs for $g_{\mathrm{SI}} \approx 0.5615\,\mathrm{mS/cm^2}$. Figure 4 illustrates the result from a continuation of the 2PBVP (3.2)–(3.6) with g_{SI} increasing from $0.5\,\mathrm{mS/cm^2}$. Here, we plot the part where the response changes dramatically, while the increase in $g_{\mathrm{SI}} \approx 0.5615\,\mathrm{mS/cm^2}$ is only of order $O(10^{-7})$. Since AUTO takes many continuation steps to capture this variation in the response, we plot the total integration time T_{OFF} in Figure 4(a) versus the point number of the continued branch. To illustrate the deformation of the response during spike adding, we select eleven solutions along the continuation branch and plot in Figure 4(b) their corresponding time series in V using a blue colour gradient from dark to light as $g_{\mathrm{SI}} \approx$

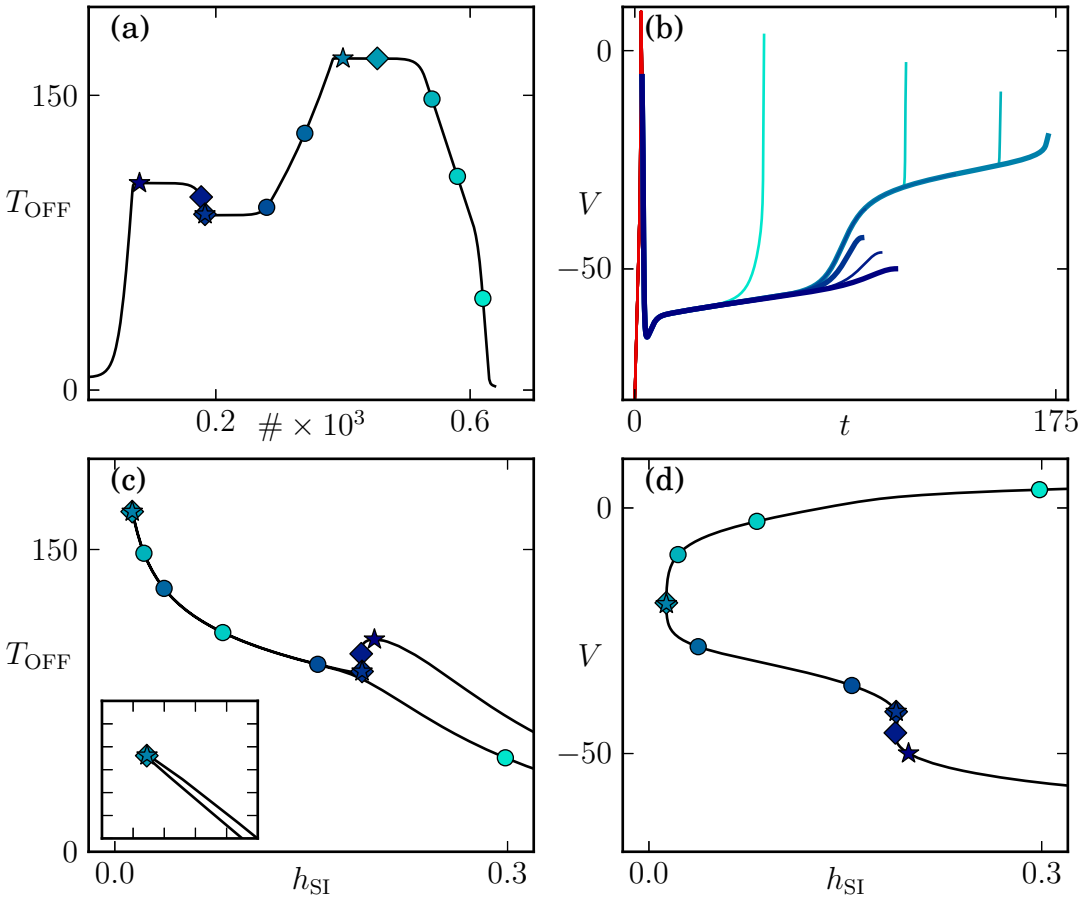

Figure 4: Continuation of the 2PBVP (3.2)–(3.6) as g_{SI} increases over an exponentially small parameter interval with $g_{\mathrm{SI}} \approx 0.5615\,\mathrm{mS/cm^2}$. Panel (a) shows the solution branch of the g_{SI}-dependent family with T_{OFF} on the vertical axis and the point number # along the branch (in thousands) on the horizontal axis; time series for V of selected orbit segments marked in panel (a) are visualized in panel (b). The extremal orbit segments with respect to the T_{OFF} are marked by stars in panel (a) and shown with thicker lines in panel (b). Panel (c) shows the same solution branch, as in panel (a), but with the h_{SI}-coordinate at the end points $\mathbf{u}_{\mathrm{OFF}}(1)$ on the horizontal axis; this panel illustrates that the extrema of T_{OFF} are located at almost the same points where h_{SI} at $\mathbf{u}_{\mathrm{OFF}}(1)$ is at a local minimum or maximum (marked by a diamonds). The inset in panel (c) highlights the smooth behaviour near the global maximum for T_{OFF}. Panel (d) shows the end points $\mathbf{u}_{\mathrm{OFF}}(1)$ in projection onto the (h_{SI}, V)-plane and gives a better idea of the overall smoothness of the solution branch; again the colour gradient along the marked solutions serves as a guide how g_{SI} increases along the branch.

$0.5615\,\mathrm{mS/cm^2}$ increases. The continuation branch in Figure 4(a) contains three extrema where the derivative with respect to T_{OFF} vanishes (marked by stars); the corresponding solutions are shown with thicker lines in panel (b). The orbit segment with the smallest selected g_{SI}-value has a local maximum with respect to T_{OFF} at $T_{\mathrm{OFF}} \approx 105.3808\,\mathrm{ms}$. Its time series is the bottom (darkest blue) curve in Figure 4(b) shown with a thicker line to indicate that T_{OFF} is at an extremum here. As g_{SI} increases, the next two solutions have smaller T_{OFF}-values, but we observe in Figure 4(b) that the V-value at the end point $\mathbf{u}_{\mathrm{OFF}}(1)$ rises; note that our selection includes the second extremal solution, where T_{OFF} has a local minimum. The voltage at $\mathbf{u}_{\mathrm{OFF}}(1)$ continues to rise slowly as we follow the branch in Figure 4(a) up to the maximum $T_{\mathrm{OFF}} \approx 168.8113\,\mathrm{ms}$, which is again indicated by a thicker line in Figure 4(b). As expected, the time series of solutions that are selected for values of $g_{\mathrm{SI}} \approx 0.5615\,\mathrm{mS/cm^2}$ past this maximum exhibit a well-defined spike, that is, they exhibit a substantial rise in V over a relatively short time interval.

Unfortunately, the numerical detection of a maximum in T_{OFF} can be computationally difficult, because there is no *a priori* bound on T_{OFF}. We have found a different approach that is numerically very stable and detects the onset of a spike at virtually the same g_{SI}-value. The substantially longer duration of the depolarised state allows the slow inward current I_{SI} to inactivate almost completely. Figure 4(c) shows the same solution branch as in Figure 4(a), but instead of g_{SI}, we plot the h_{SI}-coordinate at the end points $\mathbf{u}_{\mathrm{OFF}}(1)$ on the horizontal axis. We observe that the inactivation h_{SI} of I_{SI} appears to reach a minimum exactly when T_{OFF} achieves its maximum. As for T_{OFF}, there are three extrema for the h_{SI}-coordinate at $\mathbf{u}_{\mathrm{OFF}}(1)$, which are marked by diamonds in Figure 4, and all three are close to the three extrema for T_{OFF} (marked by stars); in fact, one can only distinguish nine different solutions in Figure 4(b), because two of the extrema with respect to the h_{SI}-coordinate at $\mathbf{u}_{\mathrm{OFF}}(1)$ are virtually identical to extrema with respect to T_{OFF}. The solution branch for the continuation of system (3.2)–(3.6) with g_{SI} increasing from $0.5\,\mathrm{mS/cm^2}$ to $0.6\,\mathrm{mS/cm^2}$ is perhaps best visualized in projection of the end points $\mathbf{u}_{\mathrm{OFF}}(1)$ onto the (h_{SI}, V)-plane as shown in Figure 4(d); g_{SI} increases from the bottom right to the top right in this picture and the extrema for T_{OFF} and h_{SI} are again marked by stars and diamonds, respectively. The spiking threshold, which is defined by the fact the T_{OFF} is globally maximal, can be viewed as the point where h_{SI} at $\mathbf{u}_{\mathrm{OFF}}(1)$ is minimal, which numerically occurs at the same value $g_{\mathrm{SI}} \approx 0.5615\,\mathrm{mS/cm^2}$ with a difference of $O(10^{-8})$. Numerically, it is advantageous to detect the global minimum of h_{SI} at the end point $\mathbf{u}_{\mathrm{OFF}}(1)$, because the h_{SI}-coordinate at $\mathbf{u}_{\mathrm{OFF}}(1)$ is biophysically restricted to the interval $[0, 1]$ and cannot grow unboundedly. As shown in Figure 4, not only the g_{SI}-value, but also the corresponding value for V at $\mathbf{u}_{\mathrm{OFF}}(1)$ and the total integration time T_{OFF} are very similar at this minimum of h_{SI}.

We remark here that the behaviour of the h_{SI}-coordinate at $\mathbf{u}_{\mathrm{OFF}}(1)$ is representative for the behaviour of the two slow variables h_{SI} and m_{SO} in our system, and extrema of either the h_{SI}- or the m_{SO}-coordinates at $\mathbf{u}_{\mathrm{OFF}}(1)$ can be used to detect the onset of a spike. We chose to work with the h_{SI}-coordinate, because the change of h_{SI} in the low voltage region is more profound than that of m_{SO}, which is also slightly slower; see Table 1.

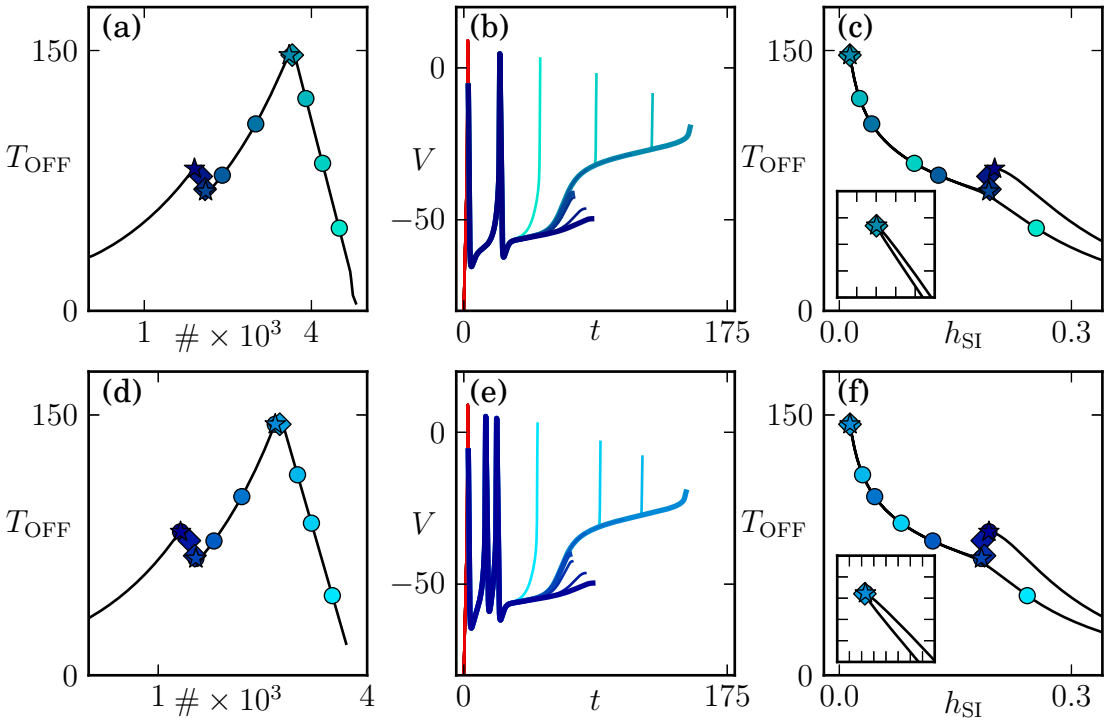

Figure 5: Continuation of families with two and three spikes that solve (3.2)–(3.6) as a function of g_{SI}. Panels (a)–(c) illustrate the branch of two-spike solutions continued past the critical threshold at $g_{\mathrm{SI}} \approx 0.5697\,\mathrm{mS/cm^2}$ and panels (d)–(f) show the branch of three-spike solutions, for which the critical threshold lies at $g_{\mathrm{SI}} \approx 0.6183\,\mathrm{mS/cm^2}$. Panels (a) and (d) show the solution branches of the g_{SI}-dependent families with T_{OFF} on the vertical axis and the point number # along the branch (in thousands) on the horizontal axis; time series for V of selected orbit segments as marked in these panels are visualized in panels (b) and (e), respectively, coloured from dark- to light-blue as g_{SI} increases (exponentially small). The extremal orbit segments with respect to the T_{OFF} are marked by stars on the solution branches and shown with thicker lines in panels (b) and (e). Panels (c) and (f) show T_{OFF} versus the h_{SI}-coordinate at the end points $\mathbf{u}_{\mathrm{OFF}}(1)$ on the horizontal axis and illustrate that these other two solution types also have the extrema of T_{OFF} located at almost the same points where h_{SI} at $\mathbf{u}_{\mathrm{OFF}}(1)$ is at a local minimum or maximum (marked by a diamonds). The insets highlight the smooth behaviour near the global maximum for T_{OFF}. Compare also with Figure 4.

For the set-up in AUTO, we solve system (3.2)–(3.6) and detect the minimum in h_{SI} at $\mathbf{u}_{\mathrm{OFF}}(1)$ using an optimization approach. To this end, we introduce a parameter denoted h^e_{OFF} and add the boundary condition

$$[0,0,0,0,1] * \mathbf{u}_{\mathrm{OFF}}(1) - h^e_{\mathrm{OFF}} = 0 \tag{3.7}$$

to system (3.2)–(3.6). Here, the vector product $[0,0,0,0,1] * \mathbf{u}_{\mathrm{OFF}}(1)$ extracts the h_{SI}-coordinate from $\mathbf{u}_{\mathrm{OFF}}(1)$. We now allow h^e_{OFF} to vary freely during the continuation; note that T_{OFF} also remains a free parameter in this 2PBVP. The advantage of such a setup is that AUTO can detect folds with respect to the parameter h^e_{OFF}; since the boundary condition (3.7) is only satisfied when h^e_{OFF} equals the value of the h_{SI}-coordinate at the end point of a solution $\{(\mathbf{u}_{\mathrm{ON}}(t), \mathbf{u}_{\mathrm{OFF}}(t)) \mid 0 \leq t \leq 1\}$ for system (3.2)–(3.6), this means that AUTO effectively detects the extrema of h_{SI} at the end point $\mathbf{u}_{\mathrm{OFF}}(1)$.

Figure 5 illustrates that our method for detecting the onset of a spike also works for solutions with more than one spike in their transient response. The next two spike generations occur over exponential small parameter intervals at $g_{\mathrm{SI}} \approx 0.5697\,\mathrm{mS/cm^2}$ and $g_{\mathrm{SI}} \approx 0.6183\,\mathrm{mS/cm^2}$; the associated continuations runs are shown in rows 1 and 2 of Figure 5, respectively. The starting solutions for these runs were found as follows. We selected two nearby solutions from the branch computed for Figure 4, namely, at $g_{\mathrm{SI}} = 0.5690\,\mathrm{mS/cm^2}$ and at $g_{\mathrm{SI}} = 0.6180\,\mathrm{mS/cm^2}$. These parameter values are well past the exponentially small g_{SI}-interval during which the second spike is generated, so that both solutions are orbit segments with one spike followed by the rising part of the next spike up to the (local) maximum. We extended these orbit segments for $g_{\mathrm{SI}} = 0.5690\,\mathrm{mS/cm^2}$ and $g_{\mathrm{SI}} = 0.6180\,\mathrm{mS/cm^2}$ by increasing T_{OFF} such that they are solutions of system (3.2)–(3.6) that exhibit two and three spikes, respectively, before ending in a local maximum of the ADP at $\mathbf{u}_{\mathrm{OFF}}(1)$. Panels (a) and (d) correspond to Figure 4(a) and show the total integration time T_{OFF} versus the point number of the continued branch. The time series in V of selected solutions as marked in panels (a) and (d) are shown in panels (b) and (e), respectively; the thicker curves indicate a solution for which T_{OFF} achieves a local maximum or minimum, which are marked by stars on the continuation branch. Figures 5(c) and (f) show the continuation branch by plotting T_{OFF} versus the h_{SI}-coordinate at the end point $\mathbf{u}_{\mathrm{OFF}}(1)$, as was done in Figure 4(c) for the one-spike solution branch. This last projection illustrates that extrema of h_{SI} at $\mathbf{u}_{\mathrm{OFF}}(1)$ (marked by diamonds) appear to be closely related to extrema of T_{OFF} (marked by stars) and the global minimum of h_{SI} at $\mathbf{u}_{\mathrm{OFF}}(1)$ is a good approximation for the global maximum of T_{OFF} that characterises the onset of the next spike.

4 Computing boundaries between transient bursting patterns

Our numerical methods for detecting the g_{SI}-values at which the system exhibits the onset of ADP or the onset of a spike are all based on detecting fold bifurcations for a 2PBVP in AUTO (Doedel, 1981; Doedel & Oldeman, 2009). This means that we can subsequently use fold continuation in AUTO to trace the onsets of APD or a spike as curves in a two-parameter plane. Such curves would form the boundaries between different bursting behaviours of the model. We illustrate this by computing the boundary curves in the $(g_{\mathrm{FO}}, g_{\mathrm{SI}})$-plane, because the magnitude of g_{FO} influences the amplitude of ADP and, thus, the overall excitabil-

ity (Nowacki et al., 2011).

There are two types of curves, namely, onset of ADP and onset of a spike. In order to compute a curve in the $(g_{\mathrm{FO}}, g_{\mathrm{SI}})$-plane that forms a separatrix between regions with and without ADP, we start from a solution of the 2PBVP (3.2)–(3.6) that has a fold with respect to g_{SI}; here, only g_{SI} and T_{OFF} are free parameters. A curve that corresponds to the onset of a new spike, on the other hand, can be started from a solution of the 2PBVP (3.2)–(3.7), where h^e_{OFF}, g_{SI} and T_{OFF} are the free parameters. We then include g_{FO} in the list of free parameters and solve the 2PBVP in AUTO with the additional constraint that the system remains at a fold point with respect to g_{SI} (for onset of ADP) or h^e_{OFF} (for onset of a new spike); the corresponding extended 2PBVP is generated automatically in AUTO.

Figure 6 shows the results of the fold continuation in the $(g_{\mathrm{FO}}, g_{\mathrm{SI}})$-plane. The bifurcation diagram is shown in panel (a) and examples of responses for parameter values in the different regions are shown in panels (b)–(m). The solid curves in Figure 6(a) are the fold continuation branches. We are only interested in the positive quadrant, $g_{\mathrm{FO}}, g_{\mathrm{SI}} \geq 0\,\mathrm{mS/cm^2}$. Furthermore, the bursting regime is bounded from above by the (dashed green) curve of Hopf bifurcations of the full system (2.1). On the other side of this Hopf curve, any short-current injection drives the system into a continuous (tonic) spiking state due to the presence of a periodic attractor. For reasons that we explain later, we stop the continuation when g_{FO} reaches the value $g_{\mathrm{FO}} = 17\,\mathrm{mS/cm^2}$ (dashed magenta line). The (solid) green curve corresponds to the onset of ADP; representative responses on either side of this curve in Figures 6(b) and (c) illustrate the transition from a response with no ADP to one with the distinctive hump at the end of the spike. The blue curves correspond to onsets of a new spike and the blue-to-cyan colouring indicates the increase in the number of spikes. We continued folds of bursts with one to seven spikes; representative responses from the regions where the transient burst has an even number of spikes are shown in Figures 6(d)–(g). Note that we only show the first curve of onset of ADP, because the continuation of onset of ADP for solutions that already exhibit more than one spike leads to curves that lie virtually on top of the branches corresponding to onsets of a new spike. We computed some of these additional ADP boundaries, but the other regions of responses with no ADP are so small that we decided to ignore the distinction between such regimes altogether. Note that the curves of onsets of the second and third spike lie very close together. Both curves are computed by fold continuation in AUTO, but the solutions along these two branches are very different when considered in the full solution space $(\mathbf{u}_{\mathrm{ON}}(t), \mathbf{u}_{\mathrm{OFF}}(t), h^e_{\mathrm{OFF}}, g_{\mathrm{SI}}, T_{\mathrm{OFF}}, g_{\mathrm{FO}})$. Hence, our method successfully distinguishes the two curves and establishes each boundary accurately; note that such boundary curves are much more difficult to determine using brute-force simulations.

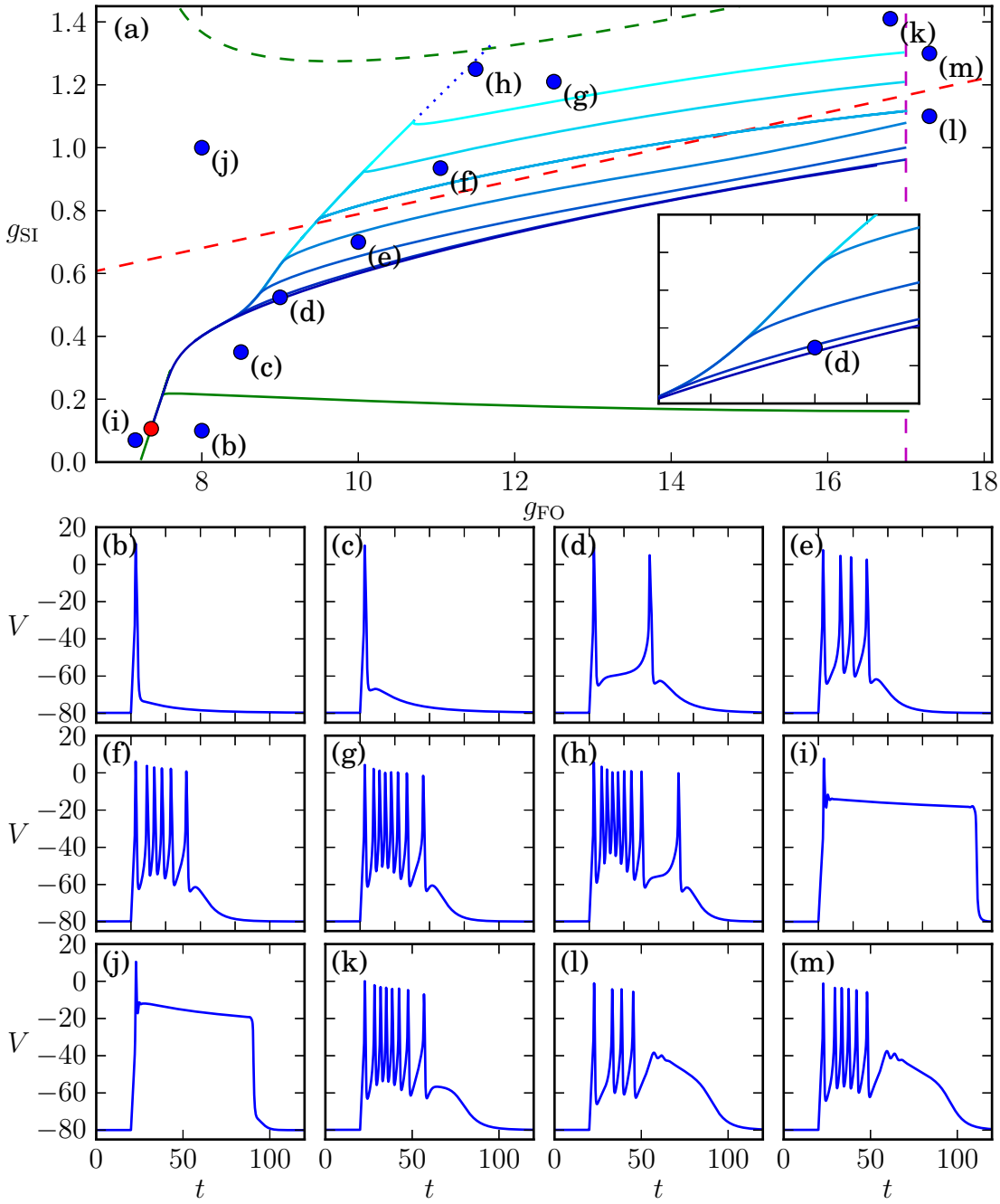

Figure 6: Regions of different model behaviour in the (g_{FO}, g_{SI})-plane established by fold continuation of system (3.2)–(3.6), or with the additional boundary condition (3.7). Panel (a) shows the bifurcation diagram, with an enlargement of the two-spike burst region in the inset, and panels (b)–(m) responses of system (2.1) for the parameter values as marked by dots in panel (a). The blue curves are the onsets of a spike, and the colour gets lighter as the number of spikes increases. The solid green curve corresponds to onset of ADP, the dashed green curve to Hopf and the dashed red curve to saddle-node bifurcation of the full system (2.1). We stopped the computations at the dashed magenta line and the red dot marks the left end point of the continuation of onsets of a spike.

The advantage of our approach is that it also successfully continues the different curves when they accumulate on each other, as is the case in the direction with g_{FO} decreasing. In fact, all seven computed curves appear to merge on the left and also merge with the (green) boundary of ADP. Again, the fold continuation in AUTO views each curve as a distinct family in the full solution space $(\mathbf{u}_{\mathrm{ON}}(t), \mathbf{u}_{\mathrm{OFF}}(t), h^e_{\mathrm{OFF}}, g_{\mathrm{SI}}, T_{\mathrm{OFF}}, g_{\mathrm{FO}})$ that is well separated from the other burst families, so that the accumulation of curves is numerically not an issue.

The continuation for each of the branches that characterise the onset of a spike stops on the boundary of ADP, approximately at the point marked by a red dot in Figure 6(a). Only the boundary of ADP extends to the g_{FO}-axis. The red dot in Figure 6(a) marks the point where the h_{SI}-coordinate at $\mathbf{u}_{\mathrm{OFF}}(1)$ reaches zero. Indeed, the curves of onsets of a spike are computed by continuation of a minimum h^e_{OFF} in the h_{SI}-coordinate at $\mathbf{u}_{\mathrm{OFF}}(1)$ and this minimum h^e_{OFF} decreases as g_{FO} and/or g_{SI} decrease. Since h_{SI} is constrained by Eq. (2.2) to the biological range $[0, 1]$, it is not possible to continue the minimum h^e_{OFF} past zero. Note that the onset of ADP takes place for much higher values of h_{SI} at $\mathbf{u}_{\mathrm{OFF}}(1)$ so that the continuation of this boundary proceeds until $g_{\mathrm{SI}} = 0$.

As mentioned above, we computed seven curves of onsets of a spike, with the last curve marking the transition between seven and eight spikes in a burst. As shown in Figure 6(a), these boundary curves accumulate in such a way that a left boundary is formed by consecutive segments of the boundary curves. We extrapolated this boundary (blue dotted line) up to the (dashed green) Hopf curve indicating the expected extent of the region with spike-adding behaviour. For example, the response in Figure 6(h) is for a $(g_{\mathrm{FO}}, g_{\mathrm{SI}})$-pair that lies very close, but to the right of this extrapolated boundary. This response is a transient burst with nine spikes, hence, there exists at least one additional curve of onset of a new spike before reaching the Hopf curve.

To the left of the (extrapolated) boundary of the spiking regime, the response is no longer a burst, but exhibits a depolarised plateau with an indistinguishable number of extremely small-amplitude spikes; two representative responses chosen far apart from each other are shown in Figures 6(i) and (j). This regime is characterised by a slow passage through a Hopf bifurcation of the fast subsystem; see (Baer, Erneux, & Rinzel, 1989; Izhikevich, 2006; Ermentrout & Terman, 2010; Desroches, Guckenheimer, Krauskopf, Kuehn, Osinga, & Wechselberger, 2012) for more details on this process. Note that this behaviour is still transient and the solution eventually returns to the resting membrane potential.

The red dashed curve in Figure 6(a) is a curve of saddle-node bifurcations of the full system (2.1); above this curve, an additional pair of equilibria coexist with the resting potential, but only the resting potential is a stable equilibrium. This curve does not act as a boundary for a particular type of bursting, but the presence of the two equilibria alters the nature of the spike-adding mechanism and T_{OFF} actually goes to infinity at the critical threshold, which is now characterised by a (transiently induced) heteroclinic connection to one of the saddle equilibria; see (Nowacki et al., 2012) for more details. While the spike-adding mechanism changes, the responses of the system on either side of the (red dashed) curve of saddle-node bifurcations inside each of the bursting regions is qualitatively the

same. Our approach for finding the onsets of a spike, where we detect a minimum for the h_{SI}-coordinate at $\mathbf{u}_{\mathrm{OFF}}(1)$ instead of a maximum for T_{OFF}, also works for $(g_{\mathrm{FO}}, g_{\mathrm{SI}})$-values above this (dashed red) curve of saddle-node bifurcations, though the solution is a coarser approximation and only the $(g_{\mathrm{FO}}, g_{\mathrm{SI}})$-values of the actual critical threshold are found accurately here.

As mentioned above, we decided to stop the computations as soon as we reached $g_{\mathrm{FO}} = 17\,\mathrm{mS/cm^2}$. For $g_{\mathrm{FO}} > 17\,\mathrm{mS/cm^2}$ the burst response develops a plateau-like ADP that contains a number of small-amplitude oscillations. The response shown in Figure 6(k), for g_{FO} just below $17\,\mathrm{mS/cm^2}$, illustrates the formation of the plateau-like ADP and Figures 6(l) and (m) are examples of what the response looks like for $g_{\mathrm{FO}} > 17\,\mathrm{mS/cm^2}$. The nature of the transient response changes in a way that is different from adding a new spike and it is more difficult to define the number of spikes in the burst. Other behaviours may arise for $g_{\mathrm{SI}} > 17\,\mathrm{mS/cm^2}$ that have not been analysed here. Note that the occurrence of small-amplitude oscillations on top of the ADP can lead to convergence problems in AUTO and it is challenging to continue the branches for larger values of g_{FO}). These numerical difficulties are due to the fact that there now exist several nearby solutions that all satisfy boundary condition (3.6), which requires that the end point $\mathbf{u}_{\mathrm{OFF}}(1)$ lies at an extremum in V. Indeed, for slightly larger T_{OFF} there exist solutions of the 2PBVP (3.2)–(3.7) that end at a minimum or maximum in V of either one of these small-amplitude oscillations; these solutions all lie close to each other, even when considering the full solution space $(\mathbf{u}_{\mathrm{ON}}(t), \mathbf{u}_{\mathrm{OFF}}(t), h^e_{\mathrm{OFF}}, g_{\mathrm{SI}}, T_{\mathrm{OFF}}, g_{\mathrm{FO}})$. Figure 6(a) gives a good overview of the sensitivity of the bursting behaviour in our model to changes in the parameters g_{SI} and g_{FO}. We find that changes in g_{SI} have a much larger effect on the bursting behaviour than changes in g_{FO}. This means that the low-voltage activated slow inward currents have larger impact on excitability in our model. We distinguish three large regimes in our region of interest: one-spike responses with ADP, one-spike responses without ADP, and the combined regions of responses with multiple spikes. As shown in Figure 6(a), the responses with just one spike and with ADP appear to cover the largest area in the parameter plane. Our simplified model has been derived based on a more detailed, biophysical model (Nowacki et al., 2011) calibrated using data from (Brown & Randall, 2009) and agrees with experimental recordings indicating that the response with just one spike followed by an ADP is the most robust (Brown & Randall, 2009). In addition, the region with no ADP after the first spike is relatively large, which is in line with the experimental results reported by Brown & Randall (2009); Golomb et al. (2006); and Yaari, Yue, & Su (2007).

5 Discussion

In this paper we presented a continuation-based numerical method for the detection of the onsets of after-depolarisation (ADP) as well as a spike in a transient burst. We defined a two-point boundary value problem (2PBVP) that identifies such onsets as special orbit segments that are determined as fold bifurcations in continuation packages such as AUTO (Doedel,

1981; Doedel & Oldeman, 2009). The 2PBVP formulation mirrors the stimulation protocols used in electrophysiological experimental studies, so that the analysis of our model can be related directly to the experimental results. We have used a relatively simple model and protocol to illustrate our approach, but our 2PBVP formulation can be adapted, in principle, to suit onsets of other phenomena in applications involving transient responses generated via different stimulation protocols. The advantage of using a model is that we can analyse the sensitivity of the model to any choice of parameters. In particular, we can make predictions for parameters that are hard if not impossible to control using experimental techniques, such as time constants or membrane capacitance.

For the detection of onset of ADP, we use the formal definition of ADP as a local maximum of the membrane potential V and defined the 2PBVP as a system for which the solutions are orbit segments that follow the stimulation protocol and end at the local maximum identifying the ADP. The disappearance of this local maximum, as a parameter is varied, occurs through an inflection point, where the local maximum merges with the preceding local minimum. During the continuation of the 2PBVP, the inflection point is detected as a fold with respect to the parameter. The onset of a spike is more challenging, because there is no parameter-independent definition of a spiking threshold. Rather than setting an arbitrary critical threshold for V, we use our findings in (Nowacki et al., 2012) that spike adding occurs via a canard-like mechanism in models of Hodgkin-Huxley type that exhibit different time scales. This means that the onset of a new spike coincides with a maximum in the time T_{OFF} that it takes the transient response to reach the local maximum of ADP as it relaxes back to the resting potential. In this paper, we argue that the drastic increase in T_{OFF}, which indicates the onset of a new spike, must be accompanied by a decrease in the inactivation h_{SI} of the slow inward current. From a numerical point of view, it is better to detect a minimum in this bounded variable h_{SI} at the end point of the orbit segment that solves our 2PBVP and we formulate it such that we can again detect this minimum as a fold point on the branch; note that this fold is not with respect to the continuation parameters.

We have shown that the detected onsets of ADP and a spike can be continued in a two-parameter plane to establish regions of different transient behaviour. Identification of such regions corresponds to a parameter sensitivity analysis of transient bursting patterns found in this class of models. Our analysis shows that there exists a large area in the parameter plane for which the response exhibits a highly depolarised state; see the responses in Figures 6(i) and (j). Similar behaviour has been observed experimentally (Golomb et al., 2006) by applying the K^+-channel blocker Linopirdine. Such a prolonged depolarised state is potentially very dangerous for the cell, because the membrane potential is away from the resting state. This may lead to excessive influx of Ca^{2+} that can reach toxic levels. We find that this region is relatively large and directly adjacent to the physiological bursts regime. Our findings indicate that hyper-excitable cells (that fire many spikes) could easily be driven into such a potentially dangerous state. We note that an increase in g_{FO} could also be dangerous, as it decreases excitability and leads to a prominent ADP with small oscillations; see the responses in Figures 6(l) and (m). Such a prolonged ADP can have a

similar effect on the influx of Ca^{2+}. Hence, this behaviour could possibly be detrimental for the cell as well.

Acknowledgements

The research for this paper was done while JN was a PhD student at the University of Bristol, supported by grant EP/E032249/1 from the Engineering and Physical Sciences Research Council (EPSRC). The research of KT-A was supported by EPSRC grant EP/I018638/1 and that of HMO by grant UOA0718 of the Royal Society of NZ Marsden Fund.

Bibliography

Andersen, P., Morris, R., Amaral, D., Bliss, T., & O'Keefe, J. (2007). *The Hippocampus Book*. New York: Oxford University Press.

Baer, S.M., Erneux, T., & Rinzel, J. (1989). The slow passage through a Hopf bifurcation: Delay, memory effects, and resonance. *SIAM J. Appl. Math.*, 49(1):55–71.

Brown, J.T., & Randall, A.D. (2009). Activity-dependent depression of the spike after-depolarization generates long-lasting intrinsic plasticity in hippocampal CA3 pyramidal neurons. *J. Physiology*, 587(6):1265–1281.

Brown, J.T., Chin, J., Leiser, S.C., Pangalos, M.N., & Randall, A.D. (2011). Altered intrinsic neuronal excitability and reduced Na(+) currents in a mouse model of Alzheimer's disease. *Neurobiology of Aging*, 32(11):, 2109.e1–2109.e14.

Dankowicz, H., & Schilder, F. (2009). CoCo*: General-purpose tools for continuation and bifurcation analysis of dynamical systems*; available via `http://sourceforge.net/projects/cocotools`.

Dankowicz, H., & Schilder, F. (2011). An extended continuation problem for bifurcation analysis in the presence of constraints. *ASME J. Comp. Nonl. Dyn.*, 6(3):031003.

Desroches,M., Guckenheimer, J., Krauskopf, B., Kuehn, C., Osinga, H.M., & Wechselberger, M. (2012). Mixed-mode oscillations with multiple time scales. *SIAM Review*, 54(2):211–288.

Doedel, E.J., & Oldeman, B.E. (2009). with major contributions from Champneys, A.R., Dercole, F., Fairgrieve, T.F., Kuznetsov, Yu.A., Paffenroth, R.C., Sandstede, B., Wang X.J., & Zhang, C.H. AUTO-07p Version 0.7: Continuation and bifurcation software for ordinary differential equations. Department of Computer Science, Concordia University, Montreal, Canada; available from http://cmvl.cs.concordia.ca/auto/.

Doedel, E.J. (1981). AUTO: A program for the automatic bifurcation analysis of autonomous systems. *Congressus Numerantium*, 30:265–284.

Elburg, R.A.J. van, & Ooyen, A. van (2010). Impact of dendritic size and dendritic topology on burst firing in pyramidal cells. *PLoS computational biology*, 6(5):e1000781.

Epsztein, J., Brecht, M., & Lee, A.K. (2011). Intracellular determinants of hippocampal CA1 place and silent cell activity in a novel environment. *Neuron*, 70(1):109–20.

Ermentrout, G.B., & Terman, D.H. (2010). *Mathematical Foundations of Neuroscience*. New York: Springer-Verlag.

Golomb, D., Yue, C., & Yaari, Y. (2006). Contribution of persistent Na^+ current and M-type K^+ current to somatic bursting in CA1 pyramidal cells: combined experimental and modeling study. *J. Neurophysiology*, 96(4):1912–1926.

Govaerts, W., & Dhooge, A. (2002). Bifurcation, bursting and spike generation in a neural model. *Int. J. Bifurcation and Chaos*, 12(8):1731–1741.

Guckenheimer, J., Gueron, S., & Harris-Warrick, R.M. (1993). Mapping the dynamics of a bursting neuron. *Philos Trans R Soc Lond, B, Biol Sci*, 341(1298):345–59.

Guckenheimer, J., & Kuehn, C. (2009). Computing slow manifolds of saddle type. *SIAM J. Appl. Dyn. Sys.*, 8(3):854–879.

Guckenheimer, J., Tien, J.H., & Willms, A.R. (2005). Bifurcations in the fast dynamics of neurons: implications for bursting. In *Bursting: The Genesis of Rhythm in the Nervous System* (pp. 89–122). Singapore: World Scientific Publishing.

Harvey, C.D., Collman, F., Dombeck, D.A., & Tank, D.W. (2009). Intracellular dynamics of hippocampal place cells during virtual navigation. *Nature*, 461(7266):941–946.

Hodgkin, A.L., & Huxley, A.F. (1952). A quantitive descritpion of membrane current and its application to conduction and excitation in nerve. *J. Physiology*, 105(117):500–544.

Hunter, J. (2007). Matplotlib: A 2D graphics environment. *Computing in Science & Engineering*, 9(3):90–95.

Izhikevich, E.M. (2000). Neural excitability, spiking and bursting. *Int. J. Bifurcation and Chaos*, 10(6):1171–1266.

Izhikevich, E.M. (2006). *Dynamical Systems in Neuroscience: The Geometry of Excitability and Bursting*. Cambridge, MA: MIT Press.

Keener, J.P., & Sneyd, J. (2008). *Mathematical Physiology: Cellular Physiology*. New York: Springer-Verlag.

Krahe, R., & Gabbiani, F. (2004). Burst firing in sensory systems. *Nature Reviews Neuroscience*, 5(1):13–23.

Kuznetsov, Yu.A. (1998). *Elements of applied bifurcation theory*. New York: Springer-Verlag.

Lee, A.K., Manns, I.D., Sakmann, B., & Brecht, M. (2006). Whole-cell recordings in freely moving rats. *Neuron*, 51(4):399–407.

Llinás, R.R. (1988). The intrinsic electrophysiological properties of mammalian neurons: insights into central nervous system function. *Science*, 242(4886):1654–1664.

Martinez-Conde, S., Macknik, S.L., & Hubel, D.H. (2002). The function of bursts of spikes during visual fixation in the awake primate lateral geniculate nucleus and primary visual cortex. *Proc. Natl. Acad. of Sciences*, 99(21):13920–13925.

McCormick, D.A., & Contreras, D. (2001). On the cellular and network bases of epileptic seizures. *Annual Review of Physiology*, 63(1):815–46.

Nowacki, J., Osinga, H.M., Brown, J.T., Randall, A.D., & Tsaneva-Atanasova, K.T. (2011).

A unified model of CA1/3 pyramidal cells: An investigation into excitability. *Progr. Biophysics and Molecular Biology*, 105(1-2):34–48.

Nowacki, J., Osinga, H.M., & Tsaneva-Atanasova, K.T. (2012). Dynamical systems analysis of spike-adding mechanisms in transient bursts. *J. Mathematical Neuroscience*, 2:7.

Oliphant, T. (2007). Python for scientific computing. *Computing in Science & Engineering*, 9(3):10–20.

Osinga, H.M., & Tsaneva-Atanasova, K.T. (2010). Dynamics of plateau bursting depending on the location of its equilibrium. *J. Neuroendocrinology*, 22(12):1301–14.

Rinzel, J. (1985). Bursting oscillations in an excitable membrane model. In *Ordinary and Partial Differential Equations*, (pp. 304–316). Berlin / Heidelberg: Springer-Verlag.

Rinzel, J. (1987). A formal classification of bursting mechanisms in excitable systems. In *Int. Congress of Mathematicians*, pp. 1578–1593.

Terman, D.H. (1991). Chaotic spikes arising from a model of bursting in excitable membranes. *SIAM J. Appl. Math.*, 51(5):1418–1450.

Terman, D.H. (1992). The transition from bursting to continuous spiking in excitable membrane models. *J. Nonlinear Science*, 2(2):135–182.

Thomas, M.J., Watabe, A.M., Moody, T.D., Makhinson, M., & O'Dell, T.J. (1998). Postsynaptic complex spike bursting enables the induction of LTP by theta frequency synaptic stimulation. *J. Neuroscience*, 18(18):7118–26.

Tsaneva-Atanasova, K.T., Osinga, H.M., Rieß, T., & Sherman, A. (2010). Full system bifurcation analysis of endocrine bursting models. *J. Theoretical Biology*, pages 1133–1146.

Tsaneva-Atanasova, K.T., Sherman, A., van Goor, F., & Stojilkovic, S.S. (2007). Mechanism of spontaneous and receptor-controlled electrical activity in pituitary somatotrophs: Experiments and theory. *J. Neurophysiology*, 98(1):131–144.

Yaari, Y., Yue, C., & Su, H. (2007). Recruitment of apical dendritic T-type Ca^{2+} channels by backpropagating spikes underlies de novo intrinsic bursting in hippocampal epileptogenesis. *J. Physiology*, 580(2):435–450.

Yue, C., Remy, S., Su, H., Beck, H., & Yaari, Y. (2005). Proximal persistent Na^{+} channels drive spike afterdepolarizations and associated bursting in adult ca1 pyramidal cells. *J. Neuroscience*, 25(42):9704–9720.

Yue, C., and Yaari, Y. (2004). KCNQ/M channels control spike afterdepolarization and burst generation in hippocampal neurons. *J. Neuroscience*, 24(19):4614–4624.